

THE STUDY AND CHARACTERIZATION OF LEAD-FREE TIN PEROVSKITE SOLAR CELL WITH HIGH EFFICIENCY USING SCAPS

M. Y. Onimisi, J.A.Ukwenya, J. A. Owolabi, U. R. Ushiekpan and A. B. Bature

Department of Physics, Nigerian Defence Academy, Kaduna, Nigeria

Abstract

In this work, a solar cell capacitance simulator (SCAPS-1D) was used in the modeling and simulation of sandwiched perovskite solar cells (PSCs) with a planar hetero-junction structure in the arrangement of the sandwiched model (FTO/CdS/CH₃NH₃SnI₃/HTM). The energy band diagram, I-V characteristics and other parameters were constructed. The configuration for better performance was then determined, from which further simulations were carried out. Results show an overall efficiency of 24.06%, FF of 83.72%, J_{SC} of 31.15mA/cm², V_{OC} of 0.92V was obtained and the electron affinity of the HTL has a great influence on the performance parameters of the solar cells with a PCE of 21.64% at 3.0eV. Tin PSC has advantage over lead free PSC because lead free is unstable due to the toxicity from lead-based PSC which does not have lead in its architecture. Hence, the p-type carrier doping concentration of tin based perovskite could improve the PCE of the device because of an enhanced built in electric field.

Keywords: Perovskite Solar Cell, numerical Simulation, SCAPS, conversion efficiency and ETM

1.0 Introduction

The development of modern trends of energy demands promising new technologies and even new physical and chemical processes for the establishment and operation of efficient systems to generate, transform and transport of energy. Today there is nothing more important than energy, since the lack of energy means a significant obstacle to the present civilization. Although global fossil fuel resources such as coal, petroleum and natural gas have not yet been exhausted, the negative social, health and environmental impacts to our current society but becoming harmful especially to the environment (environmental pollution). These permit large-scale alternative methods of producing the vast quantities of energy needed to sustain and enhance our standard of living.

To find an effective alternative for silicon-based solar cells which is the third generation solar cells, researchers in this area generally aim to provide higher efficiency at lower cost of electricity generated. The challenges vary from solar cells to solar cells, be it organic or inorganic solar cells. Basically, semiconducting materials are made from organic molecules and they possess some similarities from the first-generation and second-generation solar cells, in function but different in material. In solving the problem of organic solar cells, SCAPS-1D has been used in many simulation-based perovskite solar cells (PSCs).

Till date researchers have made efforts in contributing to the development of perovskite semiconducting materials which has led to the rise of low cost and high efficiency with respect to simulation of the solar cell capacitance simulator-one dimension (SCAPS). In 2016, [1] talks about the device simulation of lead-free CH₃NH₃SnI₃ perovskite solar cells with high efficiency. He found out that during simulation, the solar cell performance can be improved to some extent by adjusting the doping concentration of the perovskite absorption layer and the electron affinity of the buffer and HTM, while the reduction of the defect density of the perovskite absorption layer significantly improves the cell performance. By further optimizing, they obtained results of the PCE to be 23.36%, J_{SC} of 31.59mA/cm², V_{OC} of 0.92V and FF of 79.99% [1]. In 2017, high stability and reproducibility by Seok and co-workers who introduced an approach to reduce defects in the perovskite layer by using an intra-molecular exchanging process, which is favourable in reducing the defects concentration, and they obtained an efficiency of over 22% [2]. In 2018, a Comparative Study of Different ETMs in Perovskite Solar Cell with Inorganic Copper Iodide as HTM was carried out indicating Lead-based perovskite solar cell (CH₃NH₃PbI₃ PSC) with CuI as HTM, TCO, IDL and different ETMs (TiO₂, CdS, ZnSe, ZnO, ZnOS) are studied by SCAPS Simulation which show that CuI as alternate HTM has the potential to be used with perovskite absorber and can replace the Spiro-OMETAD which is expensive and suffers from degradation. The highest PCE achieved is 23.47%. The thickness of the layers has a great influence on the performance parameters of the solar cells. After optimizing the thickness of all the layers, we get a PCE of 26.11%. [3].

Cadmium sulphide (CdS) may be good alternative when used with CH₃NH₃SnI₃ absorber and cuprous oxide (Cu₂O), hole transporting material.

Corresponding Author: Onimisi M.Y., Email: myonimisi@nda.edu.ng, Tel: +2348054538199

Journal of the Nigerian Association of Mathematical Physics Volume 55, (February 2020 Issue), 139 – 152

From literatures which provides an overview and highlight the gap that the study seeks to fill, the related simulation work provides basic knowledge to develop this model [4–8]. In this architecture, we studied and analyzed the effect of thickness and doping concentration (N_A) of the absorber layer and the effect of the electron affinity of HTM and ETM on the performance of the device.

2.0 Modeling of Perovskite Solar Cell

A simple model for a planar perovskite solar cell of n-i-p device structure is used. The cross-section of this model is shown in Figure 2.1a and 2.2b. The back contact is made of silver. The cuprous oxide layer acts as the HTM and is located on top of the back contact. A p-type doped perovskite ($CH_3NH_3SnI_3$) active layer is sandwiched between the n-type material (CdS) and the p-type cuprous oxide layer. CdS is used as ETM with Fluorine doped Tin Oxide (FTO) on top.

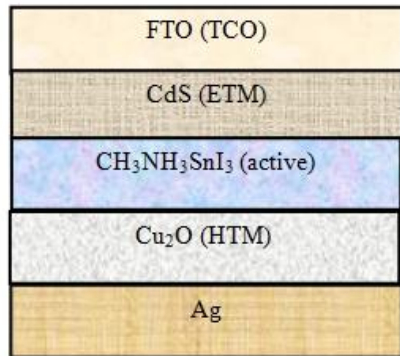


Figure 2.1a: Schematic diagram of tin perovskite solar cell

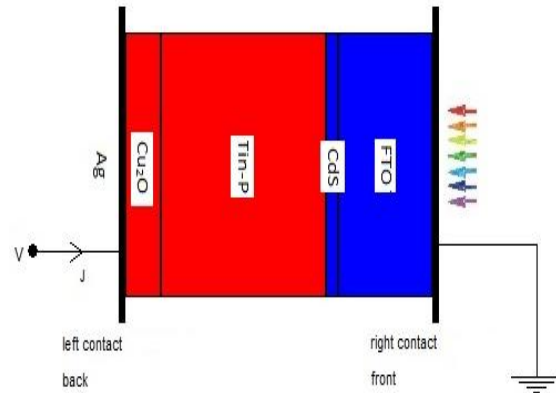
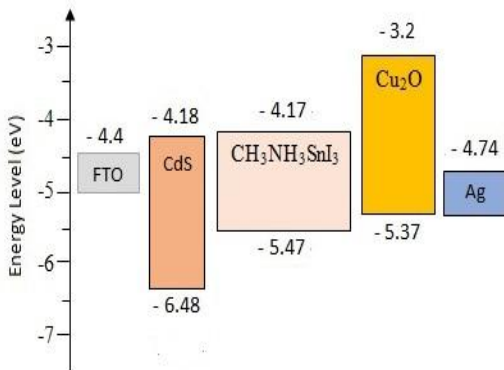


Figure 2.1b: Structure of perovskite solar cell

HTM/ $CH_3NH_3SnI_3$ and $CH_3NH_3SnI_3$ /ETM interface defect layer (IDL) are also considered to take into account the interface recombination due to interface defect density, the energy band diagram as shown in figure 2.2 indicates the conduction band offset is +0.01eV at CdS/ $CH_3NH_3SnI_3$ interface. +0.01eV signifies that the position of cadmium sulphide (ETM) layer is higher than that of the perovskite layer, which makes the electrons to migrate to the anode which is the front contact electrode. The valence band offset is +0.1eV at $CH_3NH_3SnI_3$ / Cu_2O interface, signifies that as the position of the perovskite layer is higher than that of cuprous oxide (HTM) layer which will enable high device performance and the rate of energy loss will be reduced and holes migrate to the cathode which is



back-metal contact in order to avoid their recombination

Figure 2.2: Energy band diagram

The values of device and material parameters used in SCAPS-1D for simulation that is adopted from theories and experimental data [6] are summarized in Tables 2.1 and 2.2. The work function of the cathode electrode (Ag) is 4.74eV [7] which serve as the back contact for holes transport. All the simulations will operate under the scanning voltage from 0V to 1.3V. During the simulation absorption coefficient was not used which means transmission is zero because absorption coefficient is used for optical properties and not for electrical properties. Using the optimum values of different electrical parameters found through simulation, the device performance parameters was simulated such as short-circuit current density J_{SC} , open-circuit voltage V_{oc} , fill factor FF, and power conversion efficiency PCE for different HTM-based perovskite solar cell and the final result is shown in Table 4.

Table 2.1: Device simulation parameters

Parameters	FTO	CdS	CH ₃ NH ₃ SnI ₃	Cu ₂ O
Thickness (μm)	0.4	0.05	0.7	0.15
Bandgap, E _g (eV)	3.5	2.4	1.3	2.17
Electron affinity (eV)	4.0	4.18	4.17	3.2
Relative dielectric permittivity (E _r)	9.0	10	6.5	7.11
Effective conduction band density, N _c (cm ⁻³)	2.2x10 ¹⁸	2.2x10 ¹⁸	1.0x10 ¹⁸	2.2x10 ¹⁸
Effective valence band density, N _v (cm ³)	2.2x10 ¹⁸	1.9x10 ¹⁹	1.0x10 ¹⁹	2.2x10 ¹⁸
Electron thermal velocity (cm/s)	10 ⁷	10 ⁷	10 ⁶	10 ⁷
Hole thermal velocity (cm/s)	10 ⁷	10 ⁷	10 ⁶	10 ⁷
Electron mobility, μ _n (cm ² v ⁻¹ s ⁻¹)	20	100	1.6	80
Hole mobility, μ _p (cm ² v ⁻¹ s ⁻¹)	10	25	1.6	80
Donor concentration, N _D (cm ⁻³)	10 ¹⁹	1.0x10 ¹⁸	0	0
Acceptor concentration, N _A (cm ⁻³)	0	0	3.2x10 ¹⁵	10 ¹⁸
Defect type	Neutral	Neutral	Neutral	Neutral
Capture cross section electrons (cm ²)	10 ⁻¹⁵	2.0x10 ⁻¹⁴	2.0x10 ⁻¹⁴	10 ⁻¹⁵
Capture cross section holes (cm ²)	10 ⁻¹⁵	2.0x10 ⁻¹⁴	2.0x10 ⁻¹⁴	10 ⁻¹⁵
Energetic distribution	Gauß	Gauß	Gauß	Gauß
Reference for defect energy level E _t	Above E _v	Above E _v	Above E _v	Above E _v
Energy level with respect to Reference (eV)	0.600	0.600	0.650	0.600
Characteristic energy (eV)	0.100	0.100	0.100	0.100
Defect density, N _t (cm ⁻³)	10 ¹⁵	10 ¹⁵	10 ¹⁴	10 ¹⁵

The defect layer parameter for the interface is between CdS/CH₃NH₃SnI₃[8] and CH₃NH₃SnI₃/Cu₂O [8] is summarized in Table 2.2 below.

Table 2.2: Absorber and interfaces defect parameters

Parameters	CH ₃ NH ₃ SnI ₃	CdS/CH ₃ NH ₃ SnI ₃	CH ₃ NH ₃ SnI ₃ /Cu ₂ O
Defect type	Neutral	Neutral	Neutral
Capture cross section electrons (cm ²)	2x10 ⁻¹⁴	2x10 ⁻¹⁵	1x10 ⁻¹⁸
Capture cross section holes (cm ²)	2x10 ⁻¹⁴	2x10 ⁻¹⁵	1x10 ⁻¹⁶
Energetic distribution	Gaussian	Single	Single
Energy level with respect to Reference (eV)	0.65	0.65	Above the highest Ev
Characteristic energy (eV)	0.1	0.1	0.050
Total density, N _t (cm ⁻³)	1x10 ¹⁴ -1x10 ¹⁹	1x10 ¹⁸	1x10 ¹²

III. Results and discussions

3.1. Performance of initial device parameters

This simulation result provide evidence to prove that CdS is a probable material to be used as electron transport material which has wide bandgap of 2.4eV and the simulated device performance is consistent with the experimental results of tin based PSCs [9]. Cuprous oxide has very high hole mobility, the hole mobility enhances the efficiency of CdS. Figure 3.1 shows simulated J-V curves for a CH₃NH₃SnI₃ based device in the planar electron-absorber-hole (n-i-p) configuration with Cu₂O as HTM and CdS as ETM. Cu₂O/CdS cell has high power conversion efficiency (PCE) of 17.78% with a high open circuit voltage (V_{OC}) of 0.86V, short circuit current density (J_{SC}) of 30.94 mA/cm² and high fill factor (FF) of 66.32% which is the performance for the initial device respectively.

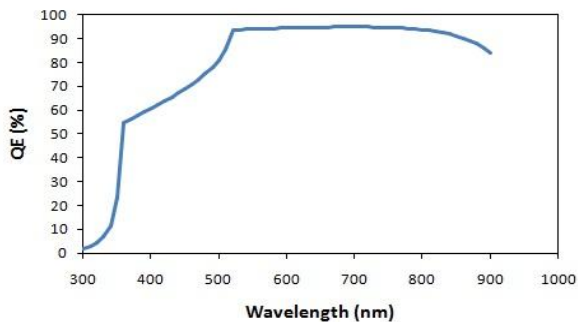


Figure 3.1: J-V curves with initial device parameters

Figure 3.2 shows the quantum efficiency (QE) of the cell featured with a high platform between 300nm and 910nm with the maximum of 94% at 700nm. In SCAPS, QE is the external quantum efficiency (EQE). The reason for this curve from 66% to 94% at 350nm to 540nm is as a result of the movement of charge carriers was not stable due to less photo sensitivity at that particular point. QE is the ratio of the number of carriers collected by the device (solar cell) to the number of photons of a given incident energy on the device. Figure 3.2: QE curves of PSC with initial parameters

3.2. Influence of thickness of absorber material

To confirm the optimum thickness of absorber layer, simulation has been carried out in the range of 0.03 to 1.5µm while other parameters are kept constant. Absorber layer thickness variation affects the diffusion length of carriers because if the absorber layer thickness is too low, absorption rate decreases, ultimately efficiency also decreases. Similarly, if the absorber layer thickness is too high, then the charge carriers may not travel up to the charge collection layers which result to decrease in the efficiency at 1.2µm as shown in table 3.2. Table 3.2 shows that an increase in thickness of absorber layer means we are increasing the light absorbed which could result in an increase in PCE and J_{SC} but FF decreases resulting to increase in charge carriers and increase in J_{SC} which could improve the PCE gradually while V_{OC} increases gradually but decrease at 0.88V from the thickness of 1.2µm since more charge carriers will not be far away from the surface which is a recombination site. The simulated parameters such as PCE, FF, J_{SC} , V_{OC} of the $CH_3NH_3SnI_3$ solar cells, with varying perovskite thickness as shown in figure 3.3a, figure 3.3b, figure 3.3c and figure 3.3d. The maximum PCE of 19.82%, with J_{SC} of 32.91mA/cm², FF of 67.44%, V_{OC} of 0.89V is achieved when the thickness reaches 0.9µm.

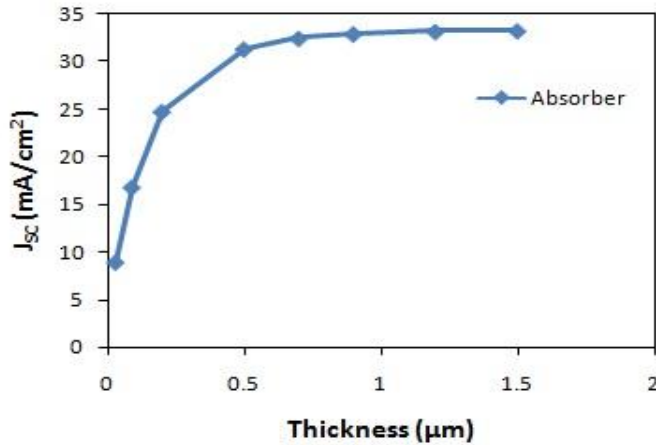


Figure 3.3b: Variation of output circuit voltage with Absorber thickness

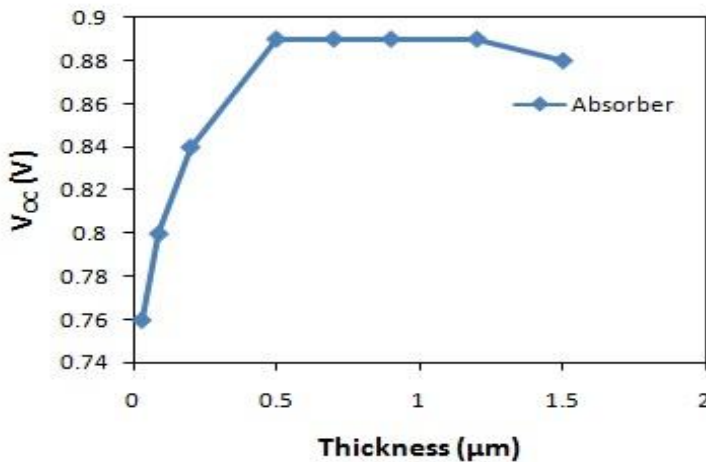


Figure 3.3a: Variation of short circuit current density with Absorber thickness

Figure 3.3c: Variation of fill factor with Absorber thickness

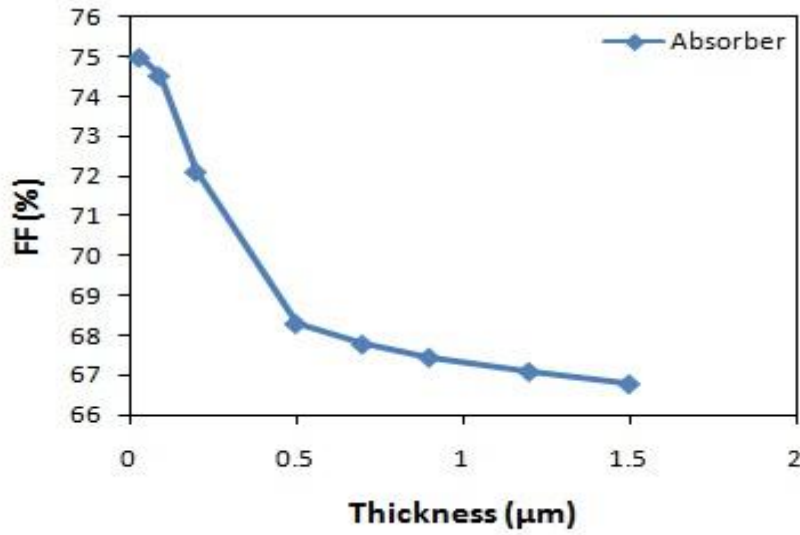


Figure 3.3d: Variation of efficiency with Absorber thickness

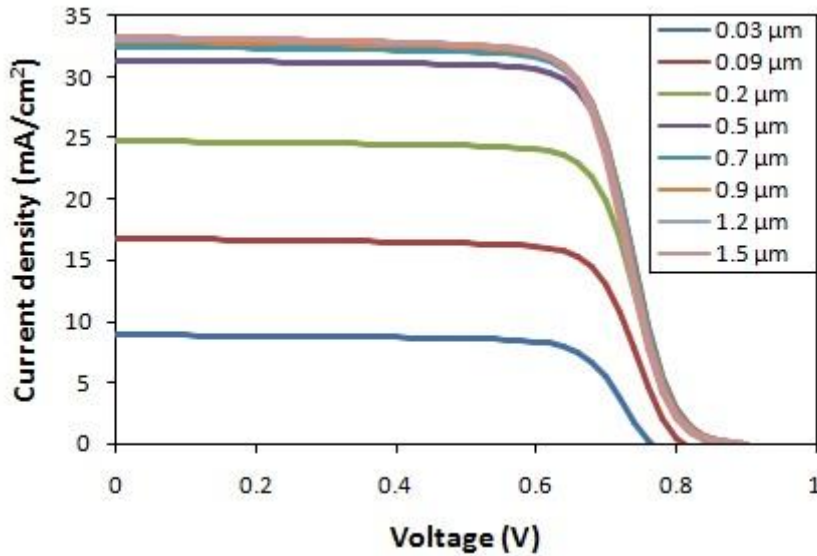


Figure 3.4: Variation in J-V curves of PSC with Absorber thickness

Table 3.1: Dependence of solar cell performance on absorber material

Absorber thickness (μm)	J_{sc} (mA/cm ²)	V_{oc} (V)	FF (%)	PCE (%)
0.03	8.87	0.76	74.99	5.08
0.09	16.76	0.80	74.53	10.11
0.2	24.73	0.84	72.11	15.15
0.5	31.32	0.89	68.29	19.08
0.7	32.44	0.89	67.77	19.65
0.9	32.91	0.89	67.44	18.82
1.2	33.16	0.89	67.08	19.81
1.5	33.23	0.88	66.77	19.71

3.3. Influence of electron affinity of ETM

The electron affinity of CdS (ETM) has been varied from 3.8eV to 4.24eV. The band offset can be adjusted because the critical factor between CdS/absorber layers is band offset as shown in figure 2.2 energy band diagram which determines the rate of carrier recombination at the interface and determines the open circuit voltage (V_{OC}). In table 3.2 the variation of electron affinity with the solar cell parameters results to decrease in J_{SC} , V_{OC} , FF and PCE due to the proper selection of an ETM with suitable electron affinity restrains the rate of carriers recombination to enable good performance of the cell. Upon optimizing the values of electron affinity of ETM at 3.8eV, J_{SC} of 31.80mA/cm², V_{OC} of 0.91V, FF of 68.51% and PCE of 19.96% were obtained as shown in figure 3.5a, figure 3.5b, figure 3.5c and figure 3.5d.

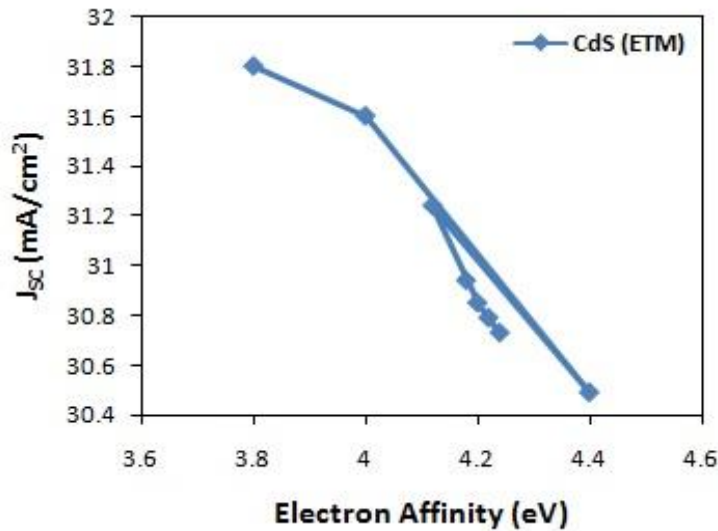


Figure 3.5a: Variation of short circuit current density with ETM electron affinity

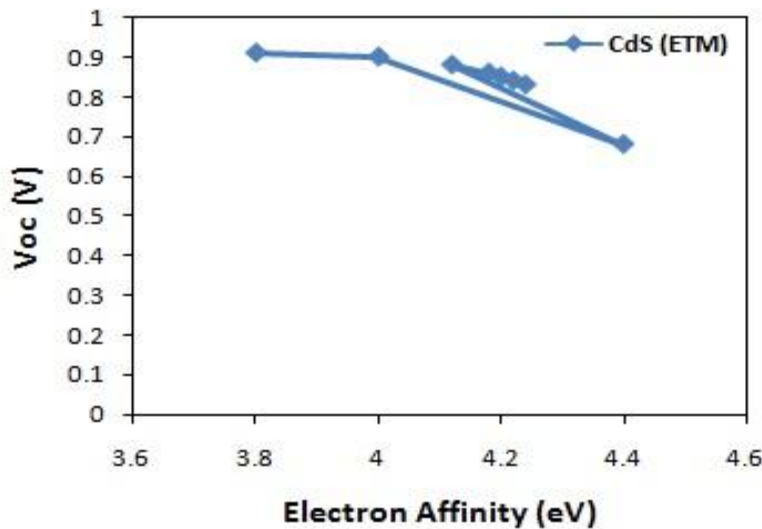


Figure 3.5b: Variation of output circuit voltage with ETM electron affinity

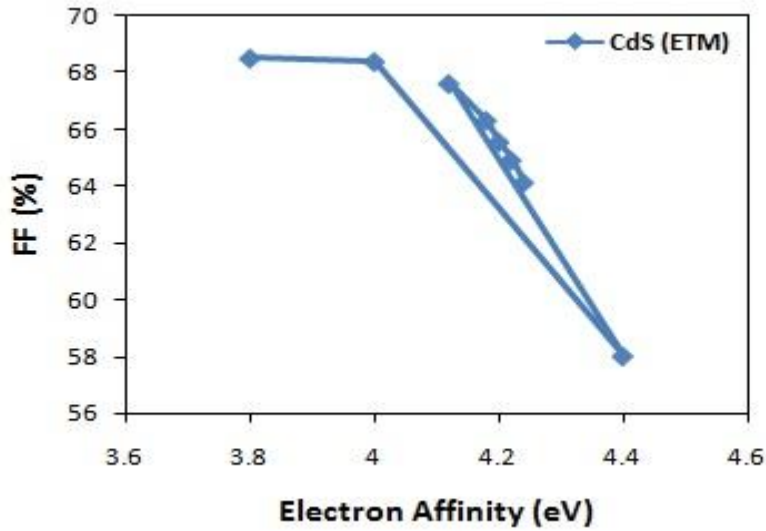


Figure 3.5c: Variation of fill factor with ETM electron affinity

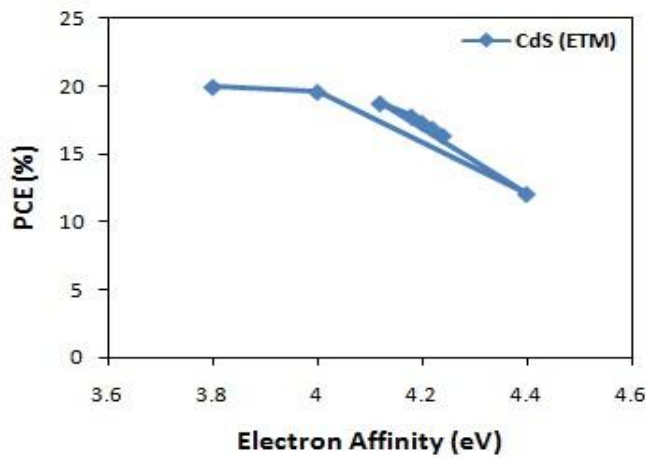


Figure 3.5d: Variation of efficiency with ETM electron affinity

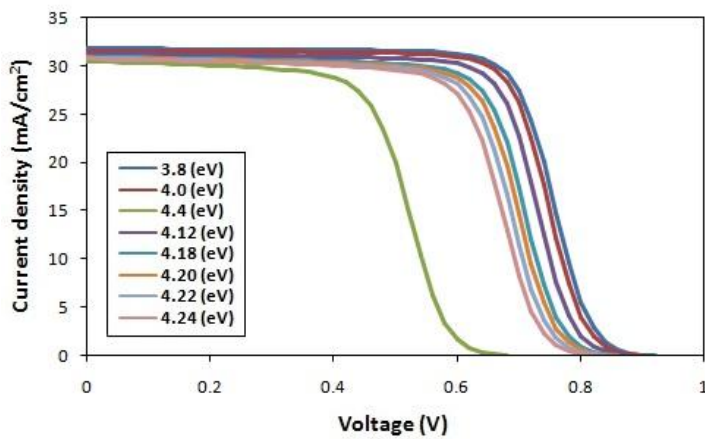


Figure 3.6: Variation in J-V curves of PSC with CdS electron affinity

Table 3.2: Dependence of solar cell performance on ETM

CdS electron affinity (eV)	J_{sc} (mA/cm ²)	V_{oc} (V)	FF (%)	PCE (%)
3.8	31.80	0.91	68.51	19.96
4.0	31.60	0.90	68.39	19.59
4.4	30.49	0.68	58.02	12.03
4.12	31.22	0.88	67.62	18.75
4.18	30.94	0.86	66.32	17.78
4.20	30.85	0.85	65.5	17.32
4.22	30.79	0.84	64.92	16.88
4.24	30.73	0.83	64.13	16.37

3.4. Influence of electron affinity of HTM

The electron affinity of Cu₂O (HTM) has been varied from 2.4eV to 3.6eV. The band offset can be adjusted because the critical factor between absorber/Cu₂O layers is band offset as shown in figure 2.2 energy band diagram which determines the rate of carrier recombination at the interface and determines the open circuit voltage (V_{oc}).When the variation of electron affinity of HTM is at 2.4eV, V_{oc} , FF and PCE are unstable but J_{sc} increases and decreases from 3.4eV. Due to the proper selection of an HTM with suitable electron affinity restrains the rate of carrier recombination to enable good performance of the cell. Upon optimizing the values of electron affinity of HTM at 3.0eV, J_{sc} of 30.97mA/cm², V_{oc} of 0.86V, FF of 80.76% and PCE of 21.64% were obtained as shown in table 3.3.

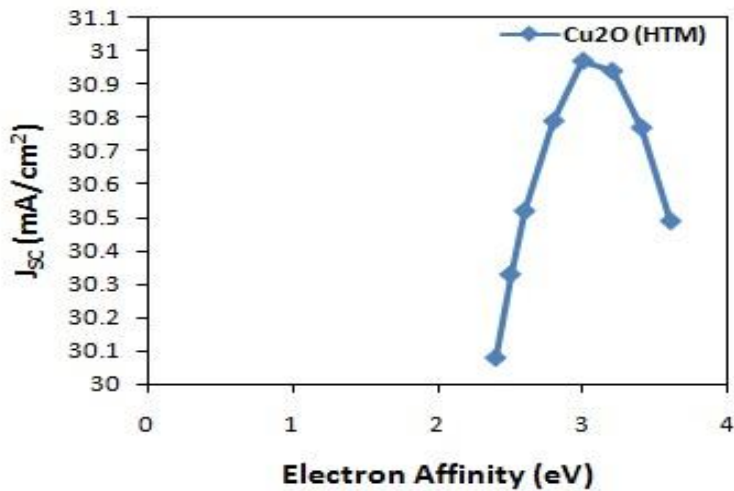


Figure 3.7a: Variation of short circuit current density with HTM electron affinity

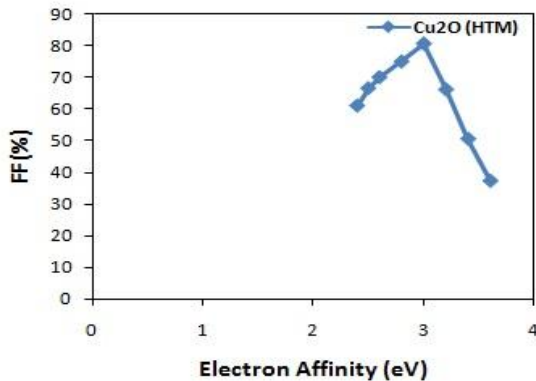


Figure 3.7b: Variation of output circuit voltage with HTM electron affinity

Figure 3.7b: Variation of output circuit voltage with HTM electron affinity

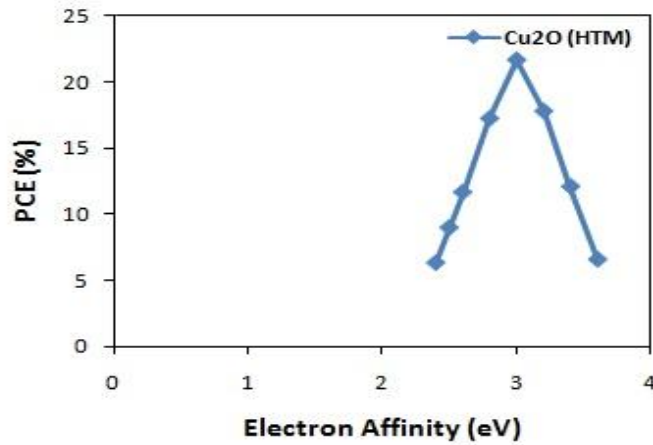


Figure 3.7c: Variation of fill factor with HTM electron affinity

Figure 3.7d: Variation of efficiency with HTM electron affinity

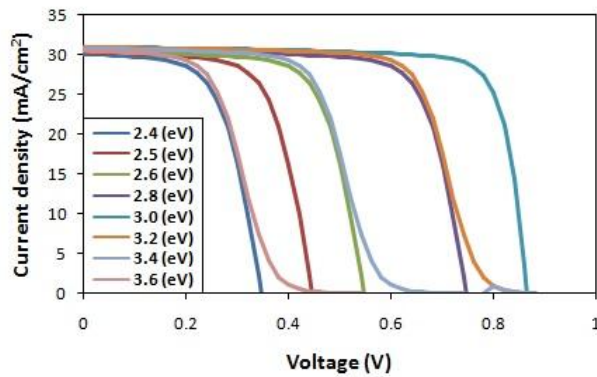


Figure 3.8: Variation in J-V curves of PSC with Cu₂O electron affinity

Table 3.3: Dependence of solar cell performance on HTM

Cu ₂ O electron affinity (eV)	J _{SC} (mA/cm ²)	V _{OC} (V)	FF (%)	PCE (%)
2.4	30.08	0.34	61.24	6.36
2.5	30.33	0.44	66.71	9.00
2.6	30.52	0.54	70.18	11.67
2.8	30.79	0.74	75.13	17.23
3.0	30.97	0.86	80.76	21.64
3.2	30.94	0.86	66.32	17.78
3.4	30.77	0.77	50.79	12.10
3.6	30.49	0.57	37.58	6.61

3.5. Influence of doping concentration (N_A) of absorber material

To enhance the performance of solar cell doping is very important. When the doping concentration of the absorber layer is varied from $3.2 \times 10^{10} \text{ cm}^{-3}$ - $3.2 \times 10^{17} \text{ cm}^{-3}$, J_{SC} increases from 29.67 mA/cm² to 31.54 mA/cm² but decreases to 31.41 mA/cm², V_{OC} decreases, FF was unstable and PCE increases from 16.15% – 17.80% but decreases to 14.58% because the p-type carrier doping concentration of tin perovskite improve the PCE of the device due to an enhanced built in electric field. Moreover, when the p-type semiconductor is doped with acceptors the Fermi energy (E_F) is pulled down to the valence energy (E_V) where we get more hole but less electrons, reverse is the case for an n-type carrier. By maximizing the carrier mobility within the active perovskite, the optimum cell performance with J_{SC} of 31.54 mA/cm², V_{OC} of 0.84V, FF of 66.79% and PCE of 17.80% is obtained as shown in table 3.4.

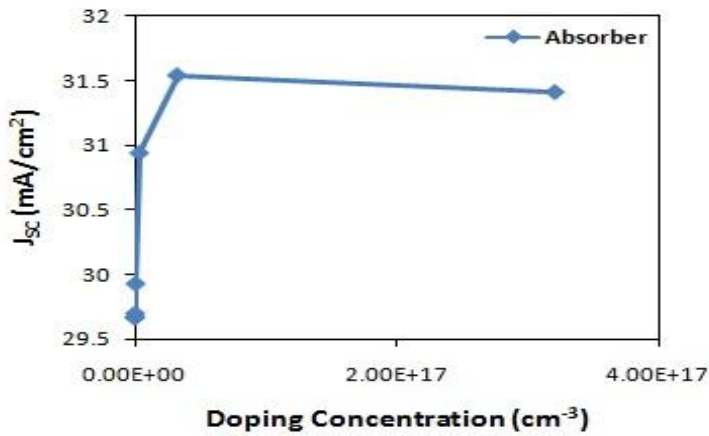


Figure 3.9a: Variation of short circuit current density with Absorber doping concentration

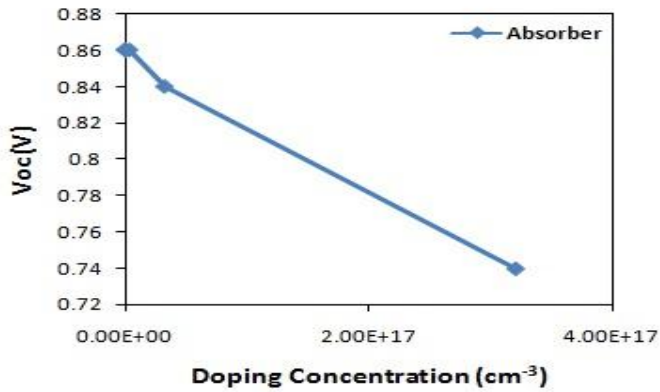


Figure 3.9b: Variation of output circuit voltage with Absorber doping concentration

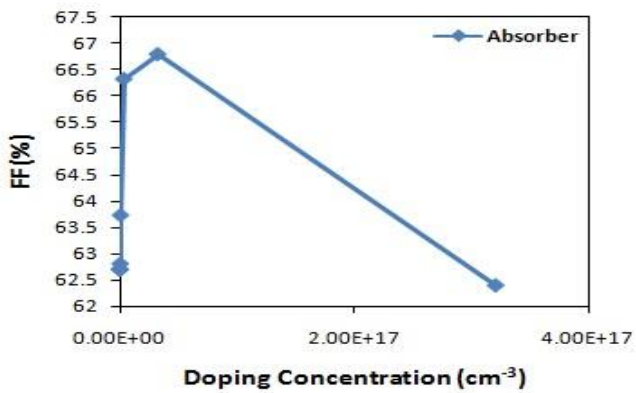


Figure 3.9c: Variation of fill factor with Absorber doping concentration

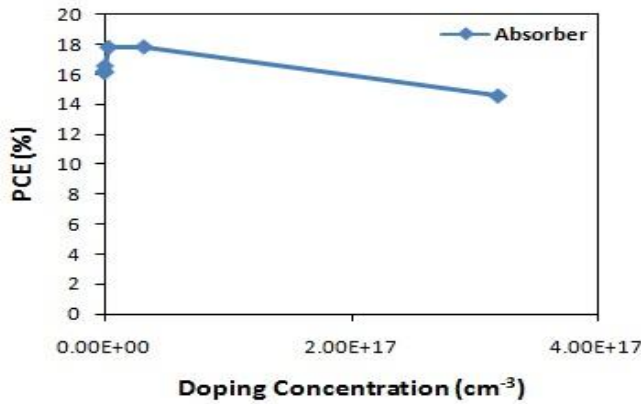


Figure 3.9d: Variation of efficiency with Absorber doping concentration

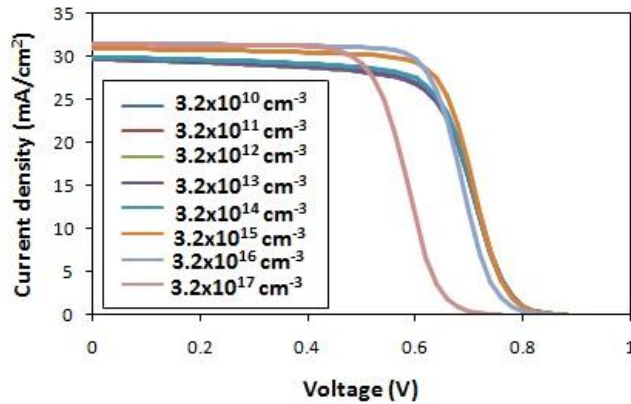


Figure 3.10: Variation in J-V curves of PSC with absorber material doping concentration

Table 3.4: Dependence of solar cell performance on absorber material

Absorber doping concentration (cm ⁻³)	J _{SC} (mA/cm ²)	V _{OC} (V)	FF (%)	PCE (%)
3.2E+10	29.67	0.86	62.71	16.15
3.2E+11	29.67	0.86	62.71	16.15
3.2E+12	29.67	0.86	62.72	16.15
3.2E+13	29.70	0.86	62.82	16.19
3.2E+14	29.93	0.86	63.74	16.55
3.2E+15	30.94	0.86	66.32	17.78
3.2E+16	31.54	0.84	66.79	17.80
3.2E+17	31.41	0.74	62.41	14.58

3.6 Performance of optimized parameters

The thickness, electron affinity and doping concentration (N_A) was considered as the following factors by which we obtain J_{SC} of 31.15mA/cm², V_{OC} of 0.92V, FF of 83.72% and PCE of 24.06%. The final optimized parameters and optimized J-V curve are shown in table 3.5 and figure 3.11 respectively. We compared our simulated results with the experiment work published by other researchers and the related data is summarized in table 3.6. The best power conversion efficiency of 6.09% has been achieved for PSCs with spiro-OMeTAD as HTM in the literature despite Cu₂O as HTM was used in this research. This could be achieved by further improving the film morphology and crystalline quality of both the absorber and spiro-OMeTAD layer. Doping of spiro-OMeTAD by replacing it with other element might or can further modify the charge carrier concentration and mobility of HTM which was done using Cu₂O in this work.

Table 3.5: Optimized parameters of the device

Optimized parameters	ETM (CdS)	Absorber (CH ₃ NH ₃ SnI ₃)	HTM (Cu ₂ O)
Thickness (μm)	---	0.900	---
Electron affinity (eV)	3.8	---	3.0
Doping concentration, N _A (cm ⁻³)	----	3.2E+16	---

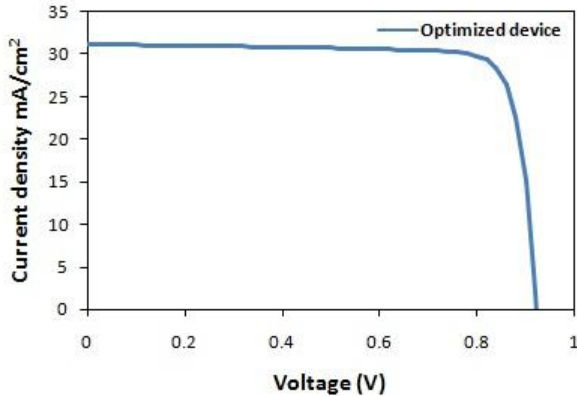


Figure 3.11: J-V curves of PSC with optimized parameters

Table 3.6: Using SCAPS to report the photovoltaic parameters of cuprous oxide based perovskite solar cells, experimental work in the literature and simulated results.

Simulation	J _{SC} (mA/cm ²)	V _{OC} (V)	FF (%)	PCE (%)
Initial	30.94	0.86	66.32	17.78
Optimized μ _m of absorber	32.91	0.89	67.44	19.82
Optimized EA of ETM	31.80	0.91	68.51	19.96
Optimized EA of HTM	30.97	0.86	80.76	21.64
Optimized N _A of absorber	31.54	0.84	66.79	17.80
Final optimization	31.15	0.92	83.72	24.06
Experimental parameters	18.67	0.68	47.43	6.09
Experimental parameters	31.59	0.92	79.99	23.36

4.0 Conclusion

In conclusion, the contribution of this study is to explore ways in which the efficiency of Sn-based perovskite can be improved. A numerical simulation approach will be used to study the characteristics of tin-based perovskite solar cells that are relevant for their performance improvement by adjusting parameters such as the thickness of absorber layer, electron affinity of ETM and HTM and doping concentration of absorber layer using SCAPS-1D. The results show that Cu₂O as HTM has the potential to be used with perovskite absorber and can replace the Spiro-OMeTAD which is expensive and suffers from degradation. CdS as an ETM can also be used to replace TiO₂ which is expensive. The highest PCE achieved is 24.06%, FF of 83.72%, J_{SC} of 31.15 mA/cm², V_{OC} of 0.92 V which is the final optimized device. The electron affinity of the HTM has a great influence on the performance parameters of the solar cells with a PCE of 21.64% at 3.0 eV.

Acknowledgements

The authors would like to say thank you to Marc Burgelman, Department of Electronics and Information Systems at the University of Gent for the development of SCAPS-1D and making it easily accessible.

REFERENCES

- [1] Du H.J., Wang W.C., and Zhu J.Z., (2016). "Device simulation of lead-free CH₃NH₃SnI₃ perovskite solar cells with high efficiency," Chinese Physics B, vol. 25.
- [2] Seok, S. I., Yang, W. S., Park, B. W., Jung, E. H., Jeon, N. J., Kim, Y. C., and Lee, D. U. (2017). Iodide management in formamidinium-lead-halide-based perovskite layers for efficient solar cells. *Science*, 356(6345), 1376-1379.
- [3] Salah M. M., Kamel M. H., Mohamed A., and Ahmed S., "A Comparative Study of Different ETMs in Perovskite Solar Cell with Inorganic Copper Iodide as HTM." *Optik* (2018), <https://doi.org/10.1016/j.ijleo.2018.10.052>

- [4] Green M.A., (1990). Photovoltaics: coming of age, Conference: Photovoltaic Specialists Conference, Conference Record of the Twenty First IEEE.
- [5] Green M.A., (1998). Solar cells: Operating principles, technology and system applications. Kensington: The University of New South Wales.
- [6] Green M.A., (2001). Solar Energy, the States of the Art. London: James & James
- [7] Gu Y.F., Du H.J., Li N.N., Yang L., and Zhou C.Y., (2019). Effect of carrier mobility on performance of perovskite solar cells. Chinese physicist B, 2019, 28(4): 048802.
- [8] Haider S. Z., Anwar H. and Wang M., (2018). “A comprehensive device modelling of perovskite solar cell with inorganic copper iodide as hole transport material”, Semiconductor Science and Technology 33035001 (2018) 12pp.
- [9] Burschka J. Pellet N., Moon S.J., Humphry-Baker R., Gao P., Nazeeruddin M.K., and Gratzel M., (2013). Sequential deposition as a route to high-performance Perovskite sensitized solar cells. Nature 499, 316–319.
- [10] Balema V., (2009). “Alternative Energy Photovoltaics, Ionic Liquids, and MOFs,” MaterialMatters, vol. 4, no. 4, p. 1.
- [11] Casas, G. A., Cappelletti, M. A., Cédola, A. P., Soucase, B. M., and Blancá, E. P. (2017). Analysis of the power conversion efficiency of perovskite solar cells with different materials as Hole-Transport Layer by numerical simulations. Super lattices and Microstructures, 107, 136-143.
- [12] Scheer R 2009 J. Appl. Phys. 105 104505
- [13] Adhikari, N., Iefanova, A. Dubey, A., Khatiwada, D., and Qiao, Q., (2016). “Lead free $\text{CH}_3\text{NH}_3\text{SnI}_3$ perovskite thin-film with p-type semiconducting nature and metal-like conductivity,” AIP Advances, vol. 6, article 085312, 2016.
- [14] Anish M., Fabian B., Jesper G.A., Fredrik H., (2016). “A review of solar Energy Based heat and power generation Systems”, Renewable and Sustainable Energy Reviews, vol. 67, pp. 1047–1064, 2017.
- [15] Backus, “Solar Cell,” IEEE Press. York, 1980.
- [16] Bansal, S., and Aryal, P., (2016). “Evaluation of new materials for electron and hole transport layers in perovskite-based solar cells through SCAPS-1D simulations,” in 2016 IEEE 43rd Photovoltaic Specialists Conference (PVSC), Portland, OR, USA, June 2016.
- [17] Behrouznejad, F., Shabbazi, S., Taghavinia, N., Wu, H.P., and Diau, E.W.G., “A study on utilizing different metals as the back contact of $\text{CH}_3\text{NH}_3\text{PbI}_3$ perovskite solar cells,” Journal of Materials Chemistry A, vol. 4, pp. 13488–13498, 2016.
- [18] Bube R.H., (1998). Photovoltaic Materials. London: Imperial College Press. Burgelman M. Nollet P., and Degraeve .S., (2000). Thin Solid Films 361, 527.
- [19] Burgelman M., Koen D., Alex N., Johan V., and Stefaan D., (2014). “SCAPS manual”.
- [20] Chen Q.Y., Huang Y., Huang P.R., Ma T., Cao C., and He Y. (2016). “Electro negativity Explanation on the efficiency-enhancing mechanism of the hybrid inorganic-organic perovskite ABX_3 from first principles study” China Physics B, DOI:10.1088/1674-1056/25/2/027104, Vol. 25, No. 2pp.027104-1-6.
- [21] Clayton, A.J.; Carlo, V.D.; Irvine, S.J.C. Investigation into ultrathin CdTe solar cell Voc using SCAPS modelling. Mater. Res. Innov. 2014, 18, 505–508.
- [22] Colegrove, E.; Blissett, C.; Buurma, C.; Ellsworth, J.; Morley, M. High-Efficiency Polycrystalline CdS/CdTe Solar Cells on Buffered Commercial TCO-Coated Glass. J. Electron. Mater. 2012, 41, 2833–2837.
- [23] Correa-Baena, J.P., Anaya, M., and Lozano G. (2016). “Unbroken perovskite: interplay of morphology, electro-optical properties, and ionic movement,” Advanced Materials, vol. 28, no. 5031, p. 7, 2016.
- [24] Cruz, L.R.; Pinheiro, W.A.; Medeiro, R.A.; Ferreira, C.L.; Dhere, R.G.; Duenow, J.N. Influence of heat treatment and back contact processing on the performance of CdS/CdTe thin film solar cells produced in a CSS in-line system. Vacuum 2013, 87, 45–49.
- [25] Du H.J., Wang W.C., and Zhu J.Z., (2016). “Device simulation of lead-free $\text{CH}_3\text{NH}_3\text{SnI}_3$ perovskite solar cells with high efficiency,” Chinese Physics B, vol. 25.
- [26] Huang L., Sun X., and Li C. (2016). “Electron transport layer-free planar perovskite solar cells: further performance enhancement perspective from device simulation,” Solar Energy Materials and Solar Cells, vol. 157, pp. 1038–1047, 2016.
- [27] Kojima, A., Teshima, K., Shirai, Y., & Miyasaka, T. (2009). Organometal halide perovskites as visible-light sensitizers for photovoltaic cells. Journal of the American Chemical Society, 131(17), 6050-6051.
- [28] Lee, M. M., Teuscher, J., Miyasaka, T., Murakami, T. N., and Snaith, H. J. (2012). Efficient hybrid solar cells based on meso-structured organometal halide perovskites. Science, 1228604.
- [29] Liu, F., Zhu, J., and Wei, J., (2014). “Numerical simulation: toward the design of high-efficiency planar perovskite solar cells,” Applied Physics Letters, vol. 104, article 253508, 2014.

- [30] Liu, P., Singh, V.P., Jarro, C.a., and Rajaputra, S., (2011). "Cadmium sulfide nanowires for the window semiconductor layer in thin film CdS–CdTe solar cells," *Nanotechnology*, vol. 22, no. 14, 2011.
- [31] Minemoto, T., and Murata, M., (2014). "Impact of work function of back contact of perovskite solar cells without hole transport material analyzed by device simulation," *Current Applied Physics*, vol. 14, pp. 1428–1433, 2014.
- [32] Sheetz, R.M.; Ponomareva, I.; Richter, E.; Andriotis, A.N.; Menon, M. Defect-induced optical absorption in the visible range in ZnO nanowires. *Phys. Rev. B Condens. Matter* 2009, 80, 195314.
- [33] Soucase, B.M., Pradas, I.G., and Adhikari, K.R., (2016). *InTech: Perovskite Materials - Synthesis, Characterisation, Properties, and Applications*, Chapter 15, 2016.
- [34] Tan, K., Lin, P., Wang, G., Liu, Y., Xu, Z., and Lin, Y., (2016) "Controllable design of solid-state perovskite solar cells by SCAPS device simulation," *Solid-State Electronic*, vol. 126, pp. 75–80, 2016.